CERAMICS AS ELECTRICAL MATERIALS

1. Introduction

Electronic ceramics materials contribute a wide range of functionalities as circuit components for microelectronics use (1,2). For most electroceramic applications the electrical conductivity, whether due to ionic, electronic, or mixed ionic–electronic conduction, is the dominant material property, that determines bulk insulation behavior. Even where the dominant material characteristic is, eg,

magnetic, ferroelectric, piezoelectric, pyroelectric, electrooptic, or electrochemical, the underlying property of primary importance for device use of these materials is electrical conduction behavior (1–5). In oxide materials such as RuO_2 and $Bi_2Ru_2O_3$, metallic conduction does occur, making them ideal for use as components in thick-film pastes and in composite electrodes. Fast ion conduction in oxide materials such as $(Zr,Y)O_{2-}$ is made use of commercially in fuel cell applications (see FUEL CELLS). Superconductivity in ceramic oxides, based on the Y–Ba and Bi–Sr–Ca cuprate structures, is being exploited for use in microwave filters and for magnetic levitation. Other classes of ceramic materials that feature semiconducting properties are used in applications as varied as resistance heating elements, rectifiers, photocells, varistors, thermistors, and sensors. Ceramic materials (qv) serve equally important functions as electrical insulators (see INSULATION, ELECTRIC). For example, glasses (qv) and porcelains (see ENAMELS, PORCELAIN OR VITREOUS) are used in both low and high voltage insulation. Alumina [1314-28-1], Al_2O_3, beryllium oxide [1304-56-9], BeO, and aluminum nitride [24304-00-5], AlN ceramics are widely used as substrates in microelectronics packaging. These materials provide added benefits of excellent thermal conduction, high mechanical strength, high corrosion resistance, and compatible thermal expansion coefficients. As substrates for microelectronic packaging, good thermal expansion match with silicon [7440-21-3], Si in order to reduce thermal stresses, low dielectric constant and loss to enhance signal processing, and high thermal conductivity for heat dissipation, are all needed characteristics. Ceramics such as silicon nitride [12033-89-5], Si_3N_4, and silicon carbide [12504-67-5], SiC, are strong, less brittle insulators, which are useful in severe environments (see ADVANCED CERAMICS, ELECTRONIC CERAMICS). For these applications, the ceramic material must also exhibit high mechanical strength, and good thermal shock resistance. Ceramics are also widely used as thin-film insulators (see THIN FILMS). Such materials as silicon dioxide [7631-86-9], SiO_2, Al_2O_3, AlN, Si_3N_4, and diamond (see CARBON–DIAMOND, SYNTHETIC), as well as several type glasses, have been developed as thin-film interlayer dielectric insulation for passivation of integrated circuit devices (see INTEGRATED CIRCUITS).

An important category of ceramic materials is that which is developed through the aliovalent doping of the insulator material to give electron conducting behavior (3–5). With controlled processing, these materials typically develop large, n-type semiconducting grains separated by thin insulating grain boundaries. This type microstructure generally results in a space charge modulated system, which features high permittivity and barrier layer capacitive behavior (3–7). Control of charge flow across the grain boundaries, through variation in temperature, can suddenly transform the material from a semiconducting to insulating state, leading to the well-known (PTCR) effect. Likewise, accelerated charge transport across the grain boundaries on application of a critical electric field, can transform the material from insulating to conducting, giving the Varistor control effect. Grain boundaries typically do not play as significant a role in NTC type thermistors, which are mainly p-type conductors in the ternary $(Mn, Ni, Fe)_3O_4$ spinel system. In this system, p-type polaron conduction occurs due to the existence of acceptor cations on the octahedral B sites (8). The activation energy for polaron hopping, however, is high, leading to a correspondingly high dependence of the conductivity on temperature. These materials, therefore,

exhibit very high temperature sensitivity and find wide usage as sensors, particularly near room temperature.

Barium titanate [12047-27-7], $BaTiO_3$ -based compounds exhibit high dielectric constants but typically must be specially formulated to satisfy specific capacitive and temperature compensating requirements (see BARIUM COMPOUNDS). They are the most widely used materials for disk, multilayer, and thick-film capacitors. More recently, relaxor-based formulations have been developed to serve both capacitive and actuator functions. These relaxors are based primarily on lead magnesium niobate (PMN), $Pb(Mg,Nb)O_3$, modified with Zn, Fe, or Ni as divalent cations and Ti, Nb, Ta, or W as higher valence cations. Important characteristics of the relaxors are their high, frequency-dependent dielectric permittivity, broad dielectric maxima, and low firing temperatures. This latter allows for cofiring in air ambient using less expensive Ag–Pd metallurgy. The trend in capacitor technology is increasingly toward integrated device packaging in which the capacitor, in thin- or thick-film form, may be embedded in the substrate (1,2). The development of ferroelectric thin films for nonvolatile memory (FeRAM) applications will likely accelerate this trend (see FERROELECTRICS). The memory films are based mainly on lead zirconate–titanate (PZT), $Pb(Ti,Zr)O_3$, formulations, either vapor deposited or sol-gel derived (see SOL–GEL TECHNOLOGY). However, other formulations, including lead titanate (PT), [12060-00-3], $PbTiO_3$, lead lanthanum zirconate titanate (PLZT), $(Pb,La)(Ti, Zr)O_3$, and relaxor compositions, have been developed for thin film use. In the bulk form, the materials are all strongly piezoelectric and rapid strides have been made in their development for use in actuator motors, ultrasonic transducers, and for electromechanical sensing (4,5). PLZT, in particular, has been widely used in electrooptic devices such as high-speed shutters, switches, light modulators and displays.

A wide range of other ceramic materials have been developed for sensor use, including gas, oxygen, temperature, voltage and humidity sensing. The sensor characteristic is typically based on the unique conduction response of oxides such as titanium dioxide [13463-67-7], TiO_2, zinc oxide [1314-13-2], ZnO, modified $BaTiO_3$, tin dioxide [18282-10-5], SnO_2, and chromium magnesium oxide [12053-26-8], $MgCr_2O_4$, to particular environmental stimulus. Because many of these sensors can provide a feedback signal for process control, ie, serve as smart sensors, these materials represent an expanding area for ceramic device application (1,2). For oxygen sensing, solid electrolyte conductors based on yttria [1314-36-9], Y_2O_3, stabilized ZrO_2 (YSZ) are the most widely used, particularly for automotive applications. Titanium dioxide is also used as an oxygen sensitive resistive sensor. Ceramic materials with mixed ionic–electronic conductivity can also be used to increase the electrocatalytic activity of the electrodes in solid oxide fuel cells (9–12). For these applications, the YSZ electrolytes are typically replaced by perovskite structure oxides, such as $LaGaO_3$, in which a wide range of oxygen stoichiometry can be developed through doping on either cation lattice site. The ionic or electronic conductivity can be readily controlled through careful processing. However, the presence of grain boundaries, which are often electronically active due to depletion effects (6), can significantly alter both the conduction and high permittivity characteristics.

Ferrites (qv) are ceramic oxides, that exhibit ferrimagnetic behavior by virtue of the opposed (A–B coupling), resulting from the presence of variable

cations on the octahedral sites within the lattice. Ferrites are widely used as inductive circuit components, including use in recording heads, microwave filters, as permanent magnets and various type induction cores (see INFORMATION STORAGE MATERIALS; MICROWAVE TECHNOLOGY). Categories of ferrite include hard, soft, and microwave materials. All are based primarily on ferric oxide [1309-37-1], Fe_2O_3. The hard ferrites are of composition $MeO{\cdot}6Fe_2O_3$, where Me = Sr, Ba, etc. This class of materials is used in permanent magnets and for motor applications. Soft ferrites, $MeO \cdot Fe_2O_3$, are based on the cubic spinel structure, where Me = Ni, Co, Cu, Zn, Li, and Mn. These cations can be readily interchanged so as to modify the magnetic permeability of the material. Ferrites are used in computer memory cores, deflection yokes, telecommunication switching and like applications. Microwave ferrites are based on the garnet structure and also contain iron oxide, eg, $3Y_2O_3{\cdot}5Fe_2O_3$. They feature high resistivity and high frequency capability. Electrical conduction can also be developed in spinel structures such as $CuCr_2O_4$, by doping with Mg^{2+} or Al^{3+} ions. These materials have been developed for use in thermoelectric power generation and the copper–nickel manganites $(Mn_{3-x-y}\ Ni_y\ Cu_x)O_4$ are used in low resistance thermistors (13).

In the oxide spinel structures cations of different valence may be distributed on octahedral or tetrahedral lattice sites, leading to electronic conduction by small polaron hopping mechanisms. In the nickel–manganites, eg, electrical conduction is due to electron hopping from Mn^{3+} to Mn^{4+} cation sites, and is controlled by dopant type and concentration (8). Similar polaron type conduction occur in the perovskite based titanates, which are used in thermistors and in high permittivity barrier layer capacitors (14–16). In these systems, cation stoichiometry is the critical factor that defines conductivity behavior, whether the mechanism be ionic, electronic or mixed (3–5).

High temperature ceramic superconductors are being developed as components in microelectronics circuitry, including thin-film devices for microwave applications, and bulk materials for various energy related storage devices (1). The structure of ceramic superconductors is based on an oxygen deficient, layered perovskite structure. Formulations in the Y–Ba–Cu–O system ($YBa_2Cu_3O_{7-x}$) have been the most widely studied, but the processing aspects needed to achieve useful shapes, controlled microstructures and high current density, remains a challenge. Many theoretical views have been put forth to account for the superconduction in these materials (17–19). An important clue has been the recognition that these materials are antiferromagnetic at low dopant concentration. From the phase diagram, there is close proximity between the antiferroelectric and superconducting phases, with antiferroelectric spin fluctuations persisting into the superconducting phase (17). It is recognized that if the spin fluctuations are coupled to the charge carriers, a high temperature transition may occur. This theory differs from the original low temperature superconductivity (BCA) theories used to explain the phenomenon, which are based on phonon interactions.

In the broad range of ceramic materials that are used for electrical applications, each category exhibits unique property characteristics that directly reflects composition, processing, and microstructure. Detailed treatment is given here primarily to those characteristics relating to insulation behavior and electrical

conduction processes. Further details concerning the more specialized electrical behavior in ceramic materials, eg, polarization, dielectric, ferroelectric, piezoelectric, electrooptic, and magnetic phenomena, are covered in (20–24).

2. Electrical Conduction

For electrical utilization, materials are usually classified according to their specific conduction mode (3–5,21,22). Insulators exhibit low carrier mobility and low conductivity, in contrast to metallic conductors, where both the carrier mobility and electrical conduction are high. Semiconductors are intermediate in conductivity, usually with exponential dependence of the conductivity on temperature. Figure 1 gives values of electrical conductivity at room temperature for a wide range of material systems. As seen from Figure 1, the electrical conductivity ranges over many orders of magnitude, from 10^5 $(\Omega\text{-cm})^{-1}$ for conducting oxides such as rhenium(VI) oxide [1314-28-9], ReO_3, and chromium(IV) [12018-01-8], CrO_2, to $10^{-14}(\Omega\text{-cm})^{-1}$ highly insulating materials such as steatite porcelains. Other compounds, such as TiO_2, may change conductivity by several orders of

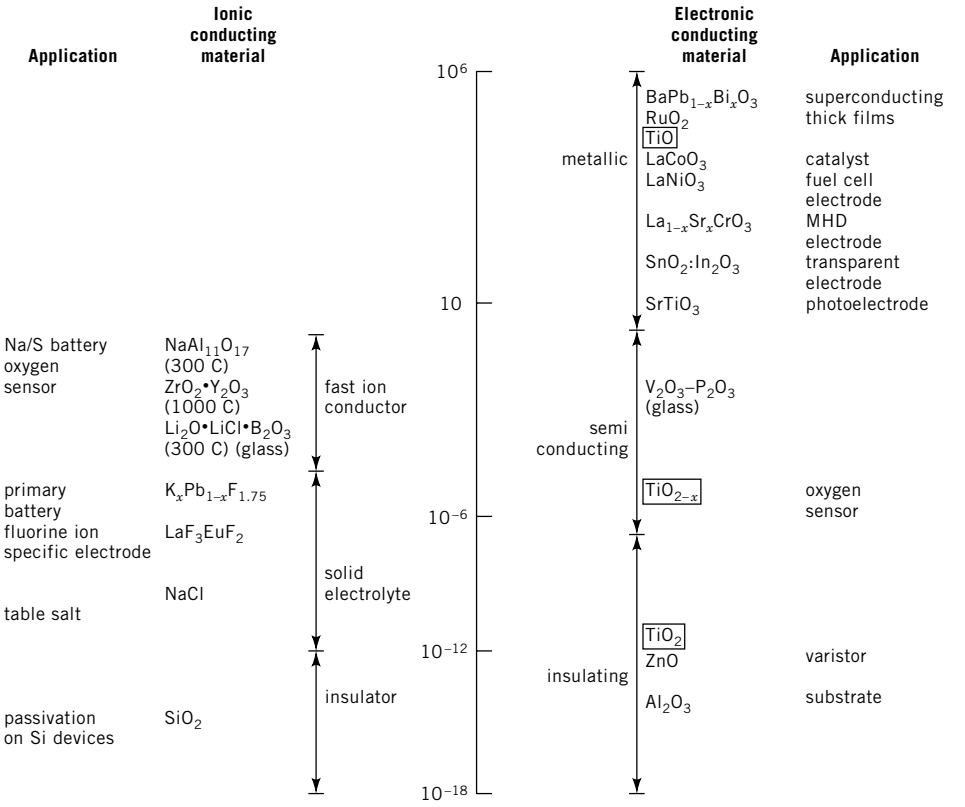

Fig. 1. Logarithmic scale of the electrical conductivities of materials categorized by magnitude and carrier type, ie, ionic and electronic, conductors. The various categories and applications are given. The wide conductivity range for the different valence–defect states of Ti oxide is highlighted. MHD is magnetic hydrodynamics.

magnitude as a result of aliovalent doping, or of high temperature heat treatment in controlled pO_2 ambient.

The charge transport mechanisms for the electrical conduction modes in ceramic materials vary greatly, since the transport of current may be due to the motion of electrons, electron holes, or ions. Crystal structure may also significantly affect the mobility of the charged species, as highlighted in Figure 1 for the various titanium oxides. The conductivity σ_i, which is associated with the mobility of the charged particles, is given as

$$\sigma_i = n_i z_i e(v_i/E) = n_i z_i^2 e^2 B_i \tag{1}$$

where n_i is the number of i particles per cubic meter, v_i is the average drift or net velocity in the direction of the applied field E, $e = 1.60 \times 10^{-19}$C, and ze is the charge on an ion of valence (z).

The conductivity term becomes complex if more than one type of charge carrier is present and involved in the conduction process. The total conductivity then becomes the sum of the fractional conductivities associated with each of the mobile carriers, be they electrons, holes or ions. This condition is represented by the expressions:

$$\sigma = \sigma_1 + \sigma_2 + \sigma_3 + \cdots + \sigma_n = \sum \sigma_i \ (i = 1 \cdots n) \tag{2}$$

The fraction of the total conductivity at a specific temperature and composition owing to the conduction of specie i is called the transference number (t):

$$t_i = \sigma_i/\sigma \tag{3}$$

where the value of t, defined as the transference number, lies between 0 and 1.0. Transference numbers for charged species in several compounds are given in Table 1, where t^+ and t^- represent the transference number for cation and

Table 1. **Transference Number of Cations t^+, Anions t^-, and Electrons or Holes $t_{e,h}$ in Several Compounds**[a]

Compound	Temperature, °C	t^+	t^-	$t_{e,h}$
AgCl	20–350	1.0		
CuCl	20	0.0		
	366	1.0		
KCl	435	0.96	0.04	
	600	0.88	0.12	
KCl + 0.02% $CaCl_2$	430	0.99	0.01	
	600	0.99	0.01	
NaCl	400	1.0		
	600	0.95	0.05	
$Na_2O{\cdot}11Al_2O_3$	<800	1.0[b]		$<10^{-6}$
$Na_2O{\cdot}CaO{\cdot}SiO_2$		1.0[b]		
BaF_2	500		1.0	
ZrO_2 + 7% CaO	>700		1.0	10^{-4}
ZrO_2 + 18% CeO_2	1500		0.52	0.48
ZrO_2 + 50% CeO_2	1500		0.15	0.85
FeO	800	10^{-4}	0.0	1.0

[a] Ref. 1.
[b] Value is for sodium ion.

anion transport respectively, and $t_{e,h}$, that for electronic transport via electrons or holes. The compound CeO_2–ZrO_2, in the system cerium(IV) oxide [1306-38-3]–zirconium oxide [1314-23-4], is an example of variable transference number occurring in an ionic system. Here, the range of ionic transference numbers for this compound can vary from 0.03 to 1.0, depending on temperature, composition and the activities of the lattice components. The electronic transference numbers are also sensitive to these factors, including also oxygen partial pressure and defect concentration.

Electrical ceramic materials are commonly used in situations where refractoriness (see REFRACTORIES) or chemical resistance is needed, or where other environmental effects may be severe. Thus, it is important to understand the effects of temperature, chemical additives, gas-phase equilibration, and interfacial reactions on the conduction behavior.

3. Ionic Conduction

For an ion to move through a crystalline lattice, there must be an equivalent vacancy or interstitial lattice site available, and it must also acquire sufficient thermal energy to surmount the free energy barrier, ΔG, between the equivalent sites. Ionic conduction, which occurs through the transport of charge by mobile ions is, therefore, a diffusion activated process. From Fick's first law, the net flux, j in the direction x for a mobile specie in a concentration gradient (dn/dx) is given by $[j = -D\ (dn/dx)]$, where the diffusion coefficient D is given by

$$D = \alpha\lambda^2\nu = \alpha\lambda^2\nu_0 e^{-\Delta G^+/kT} \tag{4}$$

Here λ is the jump distance, approximately equal to the lattice parameter spacing ($a_o \sim 3 \times 10^{-8}$cm) or to that of an adjacent plane; α is the number of possible jump sites, υ the jump frequency, υ_o the natural vibration frequency $\approx 10^{13}\text{s}^{-1}$, and ΔG is the free energy of activation. The diffusion coefficient D_i for the ionic specie i, is related to the ionic mobility by the Einstein relationship:

$$D_i = \mu_i kT/ez_i = B_i kT \tag{5}$$

These equations generally are valid for all forms of conduction. For example, to determine the flux or conductivity of ions in a solid electrolyte, as compared to electrons in a semiconducting ceramic, the parameters of interest are the concentration of charge carriers and the carrier mobility. In crystalline ceramics the charge carriers are mainly mobile ions, with different mobility values for each specie. The mobility is related to the energetics of the site-to-site transport for each type ion, but this process can be enhanced significantly by forward biasing from an applied electric field. The effect of temperature, composition and structure on each of the terms in the general expression must be considered. Equation 6, which is the Nernst–Einstein relationship, gives the conductivity for an ionic specie i with transference number, t_i,

$$\sigma_i = t_i\sigma = \left(D_i n_i z_i^2 e^2\right)/kT \tag{6}$$

The expressions for extrinsic ionic conductivity of the material, as indicated by the shortened defect notation of equation 7, show that Na^+ ion vacancies are created mainly by Ca^{2+} ion doping and not primarily generated by thermal energy.

$$Ca^{2+} \xrightarrow{NaCl} Ca_{\dot{N}a} + V_{\dot{N}a} \tag{7}$$

In ionic compounds, intrinsic thermodynamic defects, known as Frenkel or Schottky defects, are present at concentrations determined by the entropy or energy state of the solid at the given temperature. The Frenkel defect pair consists of a lattice ion on an interstitial site with associated lattice ion vacancy. This type defect typically occurs in more open structures (CaF_2, AgI), in which interstitial ions can be accommodated. Conversely, Schottky-type defects occur in close-packed structures (MgO, Al_2O_3), where both cation and anion are considered to migrate to equivalent surface sites, leaving behind cation and anion vacancies. Creation of these thermal vacancies can be expressed in terms of an equilibrium constant and, therefore, as a free energy for the formation of the defects, ΔG_f. If the ion jump is to a lattice site, then a term for the creation of vacancies must be included. This results in an added exponential term in the conductivity expression of equation 6, and is valid when the concentration of defects caused by impurities is less than that caused by thermal energy (eq. 8).

$$\sigma_i = \frac{n_i z_i^2 e^2}{kT} e^{-\Delta G^+/kT} e^{-\Delta G_f/kT} \tag{8}$$

The term $e^{-\Delta G_f/kT}$ is the probability that a site is vacant.

In nonstoichiometric and doped materials the defect structure is generally more complex. In this extrinsic region the defect concentration is nearly temperature independent, and primarily controlled by the number and valence state of the solute atoms. For many materials, temperature ranges can be found in which only one type of charge carrier, intrinsic or extrinsic, is dominant. These regions can be distinguished by different activation energies as illustrated in Figure 2, where intrinsic conduction is dominant at elevated temperatures (25).

When aliovalent, ie, different valence, impurities are added to an ionic sites, the crystal lattice compensates by forming defects that maintain both electrical neutrality and the anion to cation ratio of the host lattice. For example, addition of x mols of CaO to ZrO_2 requires the formation of x mol of oxygen vacancies.

$$x\ (CaO) \xrightarrow{ZrO_2} x\ (Ca_{Zr}) + O_O + x\ (V_O) \tag{9}$$

If this concentration is larger than the oxygen vacancies created by thermal effects, then the conductivity from the motion of the doubly charged oxygen ions will be directly proportional to the concentration of the added Ca^{2+} ions (eq. 10).

$$\sigma_{O^{2-}} = \frac{\left([CaO](2)^2 e^2\right)}{kT} e^{-\Delta G^+/kT} \tag{10}$$

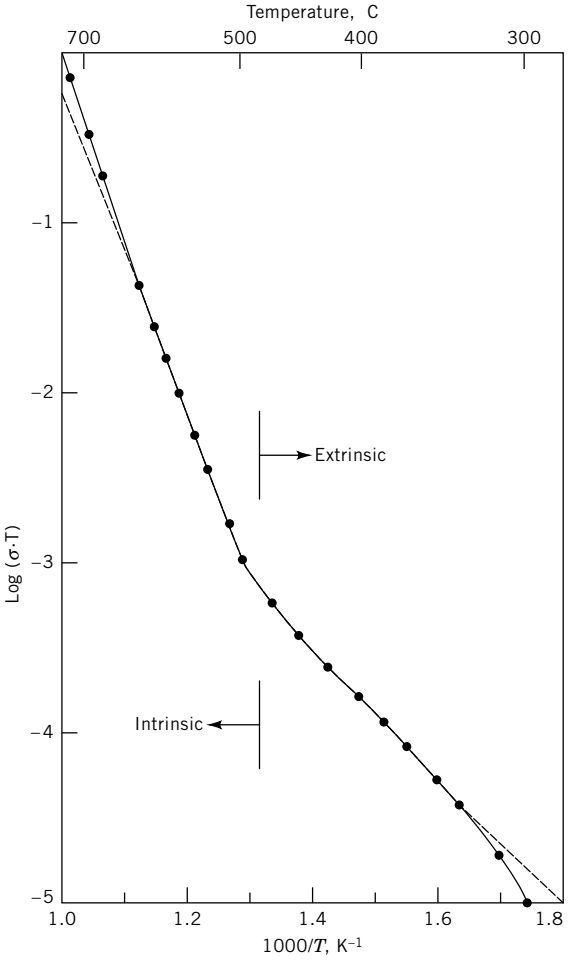

Fig. 2. Modified Arrhenius diagram of the ionic conductivity of sodium chloride. T is in kelvin, σ is in $(\Omega \cdot \mathrm{cm})^{-1}$. Over the temperature range shown the sodium ions are the primary charge carriers (25).

In polycrystalline materials, ion transport within the grain boundary must also be considered. For oxides with close-packed oxygen ions, the O^{2-} ion almost always diffuses much faster in the boundary region than in the bulk. This is due in part to second phases in the grain boundary region that are less close-packed, providing pathways for more rapid diffusion of ionic species. Thus the simplified picture of bulk ionic conduction becomes more complex when these additional effects are considered.

4. Fast-Ion Conductors

Inorganic compounds which exhibit exceptionally high ionic conductivity ($t = 1$), described as fast-ion conductors, are of technological interest for a variety of

Table 2. **Fast-Ion Conductors**

Compound	Temperature, °C	Conducting ion	σ_{ion}, $(\Omega \cdot m)^{-1}$
$NaAl_{11}O_{17}$	300	Na	35
$Na_3OZr_2PSi_2O_{12}$	300	Na	20
$CeO_2 + 12$ mol% CaO	700	O	4
$ZrO_2 + 12$ mol% CaO	1000	O	0.8
$K_{1.4}Fe_{11}O_{17}$	300	K	2
$Li_2B_4O_7$[a]	150	Li	10^{-4}
	400	Li	0.1
$Li_4B_7O_{12}Cl$[a]	300	Li	0.2
crystal	300	Li	0.8

[a] Glass.

applications, including use as solid electrolytes. As shown in Table 2, compounds in this category include: (*1*) halides and chalcogenides of silver and copper, in which the metal atoms are disordered over a large number of interstitial sites; (*2*) oxides having the β-alumina [12005-48-0], $NaAl_{11}O_{17}$, structure in which migration of the monovalent cation is aided by the presence of conduction channels, leading to high mobilities; and, (*3*) oxides of the fluorite [14542-23-5], CaF_2, structure in which a large concentration of defects can be developed through incorporation of variable valence cations, or by solid state substitution of cations of lower valence, eg, $CaO \cdot ZrO_2$ or $Y_2O_3 \cdot ZrO_2$. Conductivity values in these type compounds are many orders of magnitude larger than for normal ionic compounds and are comparable to the conductivity of such liquid electrolytes as dilute solutions of sulfuric acid.

Owing to the precise relationship between the voltage and the chemical potential gradient across the electrolyte, these materials can be used in batteries (qv), fuel cells (qv), and as ion pumps or ion-activity probes. β-Alumina, eg, is used as an electrolyte in sodium–sulfur storage batteries. The β-aluminas exhibit an hexagonal structure with approximate composition $AM_{11}O_{17}$, where A, the mobile conducting ion, is monovalent Na and the M ion is trivalent Al. The crystal structure consists of four planes of oxygen ions in a cubic close-packed array, comprising a block wherein the aluminum ions occupy some of the octahedral and tetrahedral sites between each pair of the oxygen layers, similar to the site occupancy scheme in the spinel [1302-67-6], $MgAl_2O_4$ structure. These close-packed oxygen layers or spinel-like blocks are bound together by the Na^+ ions and AlO_4 tetrahedral units. They are separated by a more open and somewhat disordered basal plane layer, consisting of oxygen ions and loosely bound Na^+ ions. This layer provides a two-dimensional (2D) pathway for rapid migration of the Na^+ ions by greater than single jump distances which, coupled with their high concentration, lead to high ionic conduction in these structures.

Some other industrially important fast ion conductor materials display both mixed electronic and ionic conduction (6,9–12,26). This group includes the $LaGaO_3$ base system in which the A and B sites are doped with a variety of ions in order to impact the defect state, creating both extrinsic ionic and electronic states. The II–III–perovskites, such as $Sr(Co,Fe)O_3$, can be excellent mixed-ion conductors and have a two orders of magnitude higher oxygen ionic conductivity than the preferred III–IV–perovskites, such as $(LaSr)(MnCo)O_3$. These materials

find use in the development of high temperature solid oxide fuel cells and sensors, where the combined effect of high electronic and ionic conduction can lead to improved electrochemical electrodes. Other uses include membranes for the production of high purity oxygen from air. The II–III based perovskite materials can develop a high concentration of ionic defects, but suffer from phase instability, which limits widespread usage (11). Doping on either the A or B site can easily change the phase transformation and temperature where electronic or ionic conductivity dominates, thereby controlling the property characteristics of these materials. Selective doping on the A or B site can retain the high electronic conductivity while increasing oxygen ion vacancy levels, and thus high ionic conductivity.

Typically, conductivity characteristics are dependent on temperature and oxygen partial pressure, hence will vary greatly depending on the degree of oxide nonstoichiometry and dopant level. The dopant level is critical since small fluctuations can lead to a decrease in electrical conductivity, oxygen nonstoichiometry, and oxygen permeation flux (10). For these mixed conducting systems, industrial applications require the avoidance of a decrease in oxygen permeation flux with time, typically associated with oxygen order–disorder phase transition in the oxygen sub–lattice. Likewise, chemical gradients can lead to strain and fracture, especially in fine separation membranes. For anode use in solid oxide fuel cells the material must exhibit high levels of mixed conduction under reducing conditions. Hence, the Ca doped $Gd_2Ti_2O_7$ pyrochlore system is attractive as an electrolyte material due to its high ionic conductivity and low electronic conductivity (12). Mo doping of this system leads to very high ionic and electronic conductivity under reducing conditions, making it suitable as an anode material. This behavior illustrates the importance of doping, which can drastically change property characteristics with only slight changes in processing parameters.

Other important fast ion conductors are the oxides having the fluorite structure, eg, ZrO_2. High (8–15 mol%) dopant levels of calcium oxide [1305-78-8] CaO or Y_2O_3 in solid solution with the ZrO_2 lead to large oxygen vacancy concentrations and vacancy ordering. The oxygen vacancies, which are produced during processing, are responsible for the high ionic conductivity in both the partially and fully stabilized zirconia. For example, for each Ca^{2+} that substitutes for a Zr^{4+} ion, an oxygen vacancy results, so that charge balance is maintained (eq. 9). Rapid oxygen migration occurs in these materials because of the high (15%) concentration of vacancies and correlated ion jumps over distances greater than the interionic separation. These structures support high oxygen ion mobility because of the low fourfold coordination of cations around the oxygens, coupled with the interconnected nature of the face-shared polyhedra that surround the oxygen sites (27). High ionic conduction results from the combination of the high oxygen vacancy concentration and high anion mobility (27). The doped ZrO_2 structures are widely used as potentiometric electrochemical sensors to detect oxygen in automotive exhausts (see EXHAUST CONTROL, AUTOMOTIVE). The sensor voltage is governed by the Nernst equation (eq. 11) where the activities are replaced by oxygen partial pressures and the air inside the chamber ($P^{II}_{O_2}$) is used as reference.

$$E = {}^{-}(RT/4F)\ln\left(P^{I}_{O_2}/P^{II}_{O_2}\right) \tag{11}$$

Here, E is the voltage across the material, F is the Faraday constant (96,487 C), and R is the gas constant (8.314 VC/K). A porous platinum electrode is used so that the oxygen can pass freely through the electrode and react with the gas sensor material. Oxygen ions move rapidly through the $ZrO_2 \cdot Y_2O_3$ electrolyte and develop a potential difference as a result of the differential oxygen partial pressure (27,28).

Ceria (CeO_2) has the cubic fluorite structure as does ZrO_2, but it is a mixed conductor (9). In CeO_2, high electronic conductivity is observed at high temperatures and low partial pressure of oxygen, due to the formation of oxygen vacancies that controls the reduction of Ce^{4+} to Ce^{3+}, leading to n-type polaron conduction. In the ZrO_2–CeO_2 system, ionic and electronic conduction can vary over a wide concentration range, producing mixed to dominant ionic or electronic conductivity. Development of superstructures in these systems can lead to sharp changes in conductivity. Fast-ion conduction may, likewise, occur in certain glasses such as silver and alkali borates, phosphates, and molybdates (29). A condition for such conduction is the existence of channels in the highly ordered sublattice, within which the ions can easily move. Fast-ion conduction also occurs in glasses, where the mechanism can be attributed to other structural factors within the amorphous solid (27).

5. Conduction in Glasses

Electrical conduction in silicate glasses at ordinary temperatures can be attributed to the migration of univalent modifier ions such as Li^+, Na^+, K^+, H^+, and OH^-, under the influence of an applied field. At more elevated temperatures ($\sim$150°C), divalent ions, eg, Ca^{2+}, Mg^{2+}, and Pb^{2+} also contribute to conduction, although their mobility is generally low (30). Conduction in glass is an activated process and thus the number of ions contributing to conduction increases with both temperature and applied field. The temperature–resistivity dependence is given as

$$\rho = [6kT/\lambda\nu\alpha(ez)n]e^{E/kT} \tag{12}$$

where ν is the natural vibration frequency ($10^{13}s^{-1}$); λ is the average jump distance [$\sim$0.8–0.9 nm; α is the number of adjacent sites ($\sim$3); n is the concentration of charge carriers; and E is the activation energy].

As the concentration n of modifier ions increase, the effect is to loosen the structure, resulting in a lowering of the activation energy E and thus freer migration of the mobile ions. The jump distance and number of available jump sites can greatly impact the mobility of the ions. When two or more mobile ionic species are present, a condition commonly referred to as the mixed alkali effect causes a reduction in the conductivity, due to mutual blocking of the migration pathways, and thus to a mutual reduction in the ion mobility (30).

Glasses typically exhibit an amorphous or random network structure with characteristic short-range order of only a few atomic spacing. The creation of structural disorder occurs during fusion of the glass and, as in lithium borate

glass, is presumed to result from the formation of a large excess of nearly equivalent sites, giving enhanced ionic mobility (29). Even though the glass structure can be described as open because of its random nature, there is no well-defined channel for conduction to occur as found in crystalline ceramics. With respect to a basic conduction mechanism, there is no general consensus that universally explains all aspects of ionic transport in glasses (31). However, application of percolation theory within the well-known random-energy model, leads to the most consistent explanation for both ac and dc conduction effects in glasses. Explanations for the observed strong dependence of ionic conductivity on composition have mainly been based on changes in the activation energy for electrical conduction (32). For alkali migration in oxide glasses this consists of two parts: the bonding energy between the mobile cation and its charge compensating center and the elastic strain energy associated with the distortion of the glass network as the ion moves from one site to another. For glasses with a high concentration of monovalent ions as charge carriers, ionic transport is determined not only by the interactions between the ions and the glass network but also between the ions themselves (33). These effects strongly influence the structure and the geometry of the transport pathways, leading to a lowering of the activation energy and increased conductivity.

6. Ceramic Insulators

Insulators are materials that offer effective resistance to current flow in an electric field, due to the very low concentration of mobile charge carriers. Important ceramic insulators such as SiO_2, Al_2O_3, mullite ($3Al_2O_3{\cdot}2SiO_2$), BeO, AlN, boron nitride (BN) [10043-11-5], and Si_3N_4 have resistivities $\sim 10^{14}$ (Ω-cm). These high values are the result of a large energy gap between a filled valence band and the next available energy level, where the promotion of an electron into a higher state is energetically unfavorable. The conductivity of these ceramics, therefore, is significantly influenced by both ionic and electronic defects. In insulating oxides, ionic defects arise from the presence of impurities of different valence from the host cation. An aluminum ion impurity substituting on a magnesium site in the MgO [1309-48-4] host lattice creates Mg vacancies.

$$x\,(Al^{3+}) \xrightarrow{MgO} x\,(Al_{Mg}^{\bullet}) + x/2\,(V_{Mg}'') \tag{13}$$

These vacancies facilitate ionic migration of Mg^{+2} ions under the influence of an electric field which is a high temperature process, however, and room temperature conductivities are very low (Table I).

Similarly, electronic conduction may arise in oxide materials from the natural loss of oxygen, which typically occur in oxides on heating to high temperatures.

$$O_O \longrightarrow \frac{1}{2}\,O_2(g) + [V_O + 2e'] \tag{14}$$

Electrons trapped at the vacancy can become partially or fully ionized, leading to weak n-type electronic conduction. Again, the conductivity is low. Conduction in

materials such as AlN and SiC occur mainly through the presence of impurities having different valence states, leading to n- or p-type conduction.

$$Al^{3+} \xrightarrow{SiC} Al_{Si} + h^{+} \qquad (p\text{-type}) \tag{15}$$

$$Si^{4+} \xrightarrow{AlN} Si_{Al} + e' \qquad (n\text{-type}) \tag{16}$$

Similar conduction mechanisms can be expected for most nitride materials, including Si_3N_4 and BN, depending on the level of impurity doping SiC, which has only a moderate band gap ($E_g = 2.8–3.2$ eV), can become semiconducting and has been developed for device use. SiC is also widely employed as heating elements for furnace applications. Electrically insulating SiC can also be fabricated using BeO dopant additions. This is an important material for laser heat sink applications because of its high thermal conducting and electrical insulating properties (see LASERS) (34).

The primary function of insulation in electrical circuits is the physical separation of conductors and the regulation or prevention of current flow between them. Ceramic insulators are used in many demanding applications where high electrical resistance is a requirement, together with other important properties such as thermal conductivity, high operating temperatures, high dielectric strength, low dielectric loss, resistance to thermal shock, environmental resistance, thermal expansion, and long-life characteristics. Insulators of this type are known as linear dielectrics. The dielectric constant is a measure of the ability of the material to store charge relative to vacuum and is a characteristic material property. In an ac field, the electrical resistivity and dielectric constant are related by the dissipation factor, which measures the energy loss per cycle. This relationship is given by

$$\sigma = \omega \epsilon_0 k' \tan \delta = 1/\rho \tag{17}$$

Where: σ = conductivity; ρ = resistivity; ω = frequency ($2\pi f$); (ε_o = permittivity of vacuum (8.85×10^{-14} F/cm); (ε_r = dielectric constant; tan δ = dissipation factor; and ε_r tan δ = dielectric loss factor = ε_r''. The dielectric strength (DS) is a measure of the maximum voltage gradient that can be impressed across the dielectric without physical degradation of its insulating properties. Ceramics that satisfy the following property criteria at 25°C are generally classified as good insulators: $\varepsilon_r \leq 30$; $\rho \geq 10^{12}\Omega$-cm; tan $\delta \leq 0.001$; DS ≥ 5.0 kV/mm; $\varepsilon_r'' \leq 0.03$.

Silicon dioxide (SiO_2) has the lowest dielectric loss properties of any inorganic material. It is commonly used in insulating fibers and in the development of electrical porcelains ($R_2O \cdot Al_2O_3 \cdot SiO_2$). These materials have high dielectric strengths with low loss and are therefore suitable for high voltage applications such as transmission line insulators, high voltage circuit breakers, and cutouts. Mullite, $3Al_2O_3 \cdot 2SiO_2$, MgO, and steatite, $MgO \cdot SiO_2$, are extensively used for high temperature electrical insulation and for high frequency insulation because of their low loss characteristics. For electrical insulating applications and heat sinks, Al_2O_3, AlN, SiC, and Si_3N_4 are the most commonly used materials. Both SiC and $Si_3 N_4$ are also industrially valuable as high temperature heat

exchangers because of high thermal conductivity and electrical insulating behavior, high hardness, durability, excellent high temperature, corrosion, and thermal shock resistance. Films of these materials, including diamond, have been developed, where the properties obtained are similar to that of the bulk materials. The conduction processes in the films mainly result from impurity and electrode injection effects, which degrades the high resistivity and dielectric properties of the materials.

7. Electronic Conduction

High electron and electron hole mobility in ceramic materials can contribute appreciably to electrical conductivity. In certain materials, metallic levels of conductivity can result while in others the electronic contribution can be very small. In all cases, the total electrical conductivity for all modes of conduction (electronic and ionic) is given by the general equation:

$$\sigma_i = \sigma(t_{\text{ionic}} + t_{\text{electronic}}) \tag{18}$$

where the total electronic conductivity is given as

$$\sigma - ne\mu_n + pe\mu_p \tag{19}$$

n and p denote the concentrations of electrons and holes, respectively, and μ_e and μ_h are the corresponding mobilities. The mobility of electrons and holes as charge carriers are generally much higher than for ionic carriers, because they are of lower mass and charge density and less confined to particular atomic sites (25). Scattering of electrons and holes occur by phonons and at point defects, dislocations, and grain boundaries. The conductivity is determined primarily by the concentration of electrons and holes, and can be described by an energy band structure (25). Figure 3 schematically illustrates the band energy configurations corresponding to metal, intrinsic semiconductor and insulator conduction. The highest energy band, which is completely filled at $T = 0$ K, is called the valence band, and the next higher band, being empty at this temperature, is the conduction band. These energy levels are separated by an energy or band gap (E_g), which normally is not occupied by electrons (25). The band gaps for several materials are given in Table 3. As shown in Figure 3, at $T = 0$ K, metallic conduction can occur in ceramic materials where there are partially filled valence bands and a corresponding overlap with the unoccupied conduction band states. When a small energy band gap is present with no overlap, semiconduction results. If a large energy gap exists the material is insulating, because the energy gap is too great to thermally promote electrons into the conduction band. Thus, with sufficient energy input, conduction occurs either by electrons being promoted into the conduction band or through the electron holes left behind in the valence band. If a semiconductor or insulator contains defects, ie, dopants, impurities, or vacancies, that have states within the band gap, as donor or acceptor levels, the result can be an increase in conduction.

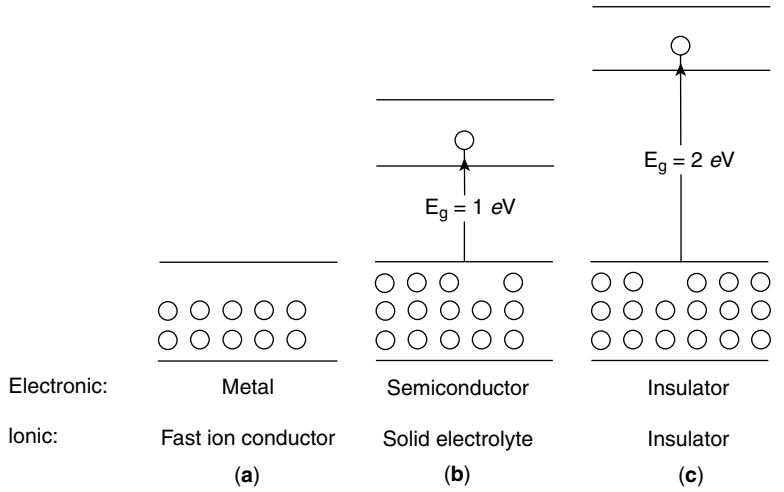

Fig. 3. Schematic of band gap energy, E_g, for the three types of electronic and ionic conductors. For electronic conductors the comparison is made of the relative occupancy of valence and conduction bands. For ionic conductors, the bands correspond to the relative occupancy of ionic sublattices. For (**a**), $n = 10^{22}\text{mL}^{-1}$ for (**b**), $n = 10^{10}\text{mL}^{-1}$; and for (**c**), $n = 1\text{mL}^{-1}$ (27).

In an ideal covalent semiconductor, electrons in the conduction band and holes in the valence band may be considered as quasifree particles. The carriers have high drift mobilities in the range of $10-10^4$ cm^2/ Vs at room temperature. As shown in Table 4, this is the case for both metallic oxides and covalent semiconductors at room temperature.

Two types of scattering may affect the motion of electrons and holes in a crystal lattice. One is lattice or phonon scattering, due to thermal vibrations within the lattice, where the vibration amplitude increases with temperature. With this enhanced vibration there is a corresponding decrease in mobility

Table 3. **Energy Gap (E_g) at Room Temperature for Intrinsic Semiconductors**

Crystal	E_g, eV	Crystal	E_g, eV
Cu_2O	2.1	Si	1.1
$BaTiO_3$	3.0–3.2	α-SiC	2.8–3.0
ZrO_2	3.2	BN	4.8
Fe_2O_3	3.4	C, diamond	5.2–5.6
ZnO	3.5		
TiO_2	3.05–3.8	AgI	2.8
CoO	4	KCl	7
BaO	5.5	CaF_2	12
CeO_2	5.5		
BeO	7.1	PbS	0.35
MgO	>7.8	GaAs	1.4
Al_2O_3	>8	GaP	2.25
SiO_2	~9	ZnS	3.6

Table 4. **Carrier Mobilities at Room Temperature**

	Mobility, $cm^2/(V \cdot s)$			Mobility, $cm^2/(V \cdot s)$	
Crystal	Electrons	Holes	Crystal	Electrons	Holes
Si	1500	450	$CoFe_2O_4$	10^{-4}	10^{-8}
diamond	1800	1200	CoO		~0.1
			NiO		~0.1
			Fe_3O_4		0.1
AgCl	50		Fe_2O_3	0.1	
KBr	100		TiO_2	0.2	
			$(BaLa)TiO_3$	0.5	0.1
AlN		10	BaO	5	
GaP	150	120	$SrTiO_3$	6	
PbS	600	200	ZnO	50	
GaAs	8500	450	SnO_2	160	

according to the relationship: $\mu \propto T^{-3/2}$. A second source of scattering arises is from impurities present at low (<100 K) temperature, which distort the periodicity of the lattice, giving a mobility relationship $\mu \propto T^{+3/2}$. The total mobility μ is proportional to the sum of these two terms. The temperature dependence of the mobility term for quasifree electrons and holes is much smaller than that for their concentration, which is exponentially determined. As a result, the conductivity has a temperature dependence determined mainly by this concentration.

Several theoretical models have been proposed to explain conduction in disordered materials, among which are the hopping and multiple trap models, as detailed by Blaise (14) and summarized briefly below. In the multiple trap model, charge transport occurs via extended states located above the mobility edge, which refers to the energy level separating localized states in the band gap from the extended or continuos states in the conduction or valence bands. In this model, the charge carriers are trapped within the band gap and released above the mobility edge, then recaptured and released many times as they progress through the material.

In the hopping model, charge transport occurs via impurity states located within the band gap. Hopping conduction is dominant when the trap energy levels are located well below the mobility edge and are populated at high concentration, such that there is an overlap of the wave functions of ions localized on the traps. The exact nature of the localized states depends on the type disorder resulting from the presence of defects such as vacancies, interstitial atoms and their ionized states. The distance between the states is in turn dependent upon the impurity concentration. A high concentration allows the localized states to overlap, with conduction occurring via thermally activated hopping between these states. The activation energy for conduction is typically < 1 eV, which allows conduction to occur at room temperature in these wide-band gap materials (14). This type conduction can be related also to charges moving from one impurity site to another via energy exchange with phonons (14–16).

In ionic host lattices where there is interaction between neighboring ions, polarization of the lattice due to the presence of an electron or hole as charge carrier, can occur. The resulting charged entity, consisting of the electronic carrier

plus its polarization field, is referred to as a polaron (16). The presence of the electron or hole in the polar material also induces a dipole. If the extension of the resultant polarization field around the electron is large compared to the distance between the unit cells in the lattice, then the concept of a discrete dipole can be replaced by that of a polarization continuum, in which there is only weak-coupling between the charge carrier and the polarization field. This is referred to as a large polaron state, in which conductivity similar to a quasifree electron state results. Large polarons are typical of III–V compounds. An intermediate polaron state is one in which the polaron radius is comparable to the unit cell, and is typical of some perovskite materials (15). In contrast, when the lattice polarization, or polaron radius, is smaller than the lattice unit cell parameter (small polaron state), the mobility becomes strongly coupled to the lattice distortion, which must move along with the electronic carrier (15,16). This process is loosely referred to as a "hopping" mechanism. The localization of the polarons is a specific case in which the polaron has a very narrow bandwidth, where the spread of energy levels due to the lattice disorder is only a few tenths of electronics. This, however, is a simplification of the mechanism since the discrete energy levels can become localized states of lower energy within the band gap (16). Polar motion then becomes possible as a result of small overlap of the wave functions of neighboring ions. Electron mobility will increase according to the degree of overlap of the partially filled local states and not through conduction bands (16). Mobility value for the small polaron is typically less than 1 cm^2/Vs) but can be much lower.

8. Electronic Conducting Ceramics

8.1. Conducting Ceramics. Metals are not the only materials that exhibit high conductivity. Metallic conduction occurs also in transition-metal oxides such as ReO_3, CrO_2, vanadium(II) oxide [12035-98-2], VO, titanium(II) oxide [12137-20-1], TiO, and rhenium(IV) oxide [12036-09-8], ReO_2 ; in doped perovskite structures such as lanthanum titanium oxide [12201-04-6], $LaTiO_3$, calcium vanadium(IV) oxide [12138-49-7], $CaVO_3$, $BaTiO_3$, strontium ferrate (1:1) [12022-69-4], $SrFeO_3$, lanthanum nickelite [12031-18-4], $LaNiO_3$, lanthanum colbaltite [12016-86-3], $LaCoO_3$, and lanthanum chromite [12017-94-6], $LaCrO_3$; in tungsten bronzes such as Na_xWO_3, La_xWO_3, and $Na_xNb_2O_5$, and in some spinels, $Li_{0.5}$ $In_{0.5}$ Cr_2 S_4, typically at specific dopant concentrations. These materials are all potentially important for fuel cell electrode use. In microelectronics, ReO_2 and RuO_2 ruthenium(IV) oxide [12036-10-1] compounds are used as the conducting phase in organic-based inks and pastes for the screen-printing of passive components in thick film circuits. The high conductivity in these transition-metal oxides typically result from overlap of unfilled *d* or *f* electron orbitals, forming energy bands with concentrations of quasifree electrons of the order of 10^{22}–$10^{23}m^{-1}$, equivalent to metallic conduction. The electronic conductivity in the perovskite and rutile oxide structures have been most studied. The electronic mobility in these simple transition-metal oxides is usually less than 1 cm^2/Vsec, leading to electrical conductivities in a broad range of [10^{-4}–10^4 $(\Omega\text{-cm})^{-1}$], with variable temperature dependencies.

Very high conduction also occurs in many ceramic materials represented by the group formula MeC_x or MeN_x, where Me is a metal, C and N are carbon and nitrogen respectively, and x is the carbon or nitrogen/metal ratio (35). These materials may exhibit covalent or ionic bonding, but with sufficient free electrons to display near-metallic behavior, including a positive and near-stable conduction with temperature. The high conductivity results from a redistribution of the orbitals and energy levels, resulting in band overlap at the Fermi energy level. TiC, for example, has no bandgap at the Fermi energy level and is, therefore, neither an insulator nor a semiconductor, but rather a metallic conductor, with resistivity values similar to the transition metals. Some of these materials, such as tantalum carbide and niobium carbide can become superconducting near 10 K (35).

8.2. Semiconducting Ceramics. Defects can be created in many ceramic materials either by controlled doping, by heat-treated under conditions which create nonstoichiometric defects, or by uncontrolled impurity doping. Since mobility values for the defect transport mechanisms are often low and difficult to measure, the conductivity values that are reported for these materials are often at variance. This is in part due to the variable effects of impurities and thermal history which often overwhelm the expected dopant effects. Both the dopants and impurities strongly influence the properties of oxide semiconductors, since the substituted ions and created defects may introduce new localized energy levels that are intermediate between the valence and conduction bands (15,16). If the new energy levels are unoccupied and lie close to the top of the valence band, electrons can be excited out of the filled valence band into the new acceptor levels, leaving behind electron holes that contribute to p-type conductivity. These p-type oxides are commonly referred to as metal deficient conductors. Conversely, if the impurity additions have filled electron energy levels close to the conduction band, electrons may be excited from these donor levels into the conduction band as n-type charge carriers. The n-type conductivity in these oxides results from a so-called metal excess in these conductors. Similar impurity dopant effects occur also in non-oxide materials such as silicon carbide, which can be doped with boron [7440-42-8] to provide acceptor levels within the band gap (0.3 eV above the valence band), thus making it a p-type conductor. Conversely, nitrogen can be added to provide donor levels below the conduction band giving n-type conduction (0.07 eV).

Strontium titanate [12060-59-2], $SrTiO_3$, can become an n-type semiconductor by donor doping of the Ti lattice sites, or by heat treatment in a reducing atmosphere with resultant loss of oxygen. Electron mobility in the doped $SrTiO_3$ is $\sim$6 cm^2/Vs. ZnO also exhibits n-type conduction when sintered under reducing conditions, since the zinc interstitials formed become electron donors, each yielding one free electron. In contrast, Copper(I) oxide [1317-39-1] is a p-type semiconductor, in which the Cu^{2+} ions or vacancies act as acceptors for electron holes that conduct within a narrow band in the Cu d orbitals. Similar to Cu_2O, Nickel monoxide [1313-99-1], NiO, forms a metal deficient semiconductor in which vacancies occur on the cation lattice sites. For each cation vacancy two electron holes must be formed, which are assumed to be associated with the regular cations ($[Ni^{2+}]\rightarrow[Ni^{3+}]$). Transfer of the positive charges between the Ni cations leads to conduction within the lattice. This type conduction is similar to

the polaron conduction described previously, where the localized states become polarized by electron hole motion. The charge-transfer process is of low mobility [0.1 cm^2 /V s], leading to relatively low conductivity of $\sim 10^{-13}(\Omega\text{-cm})^{-1}$ at 25°C, but the mobility value increases to $\sim 1(\Omega\text{-cm})^{-1}$ on doping with Li^+ ions (25). The Li^+ ions stabilize the Ni^{3+} states at a higher concentration, resulting in higher and more stable conductivity. Similarly, the insulating characteristics of NiO can be improved by doping with trivalent ions such as Cr^{3+} or Al^{3+}, which decreases the fraction of Ni^{3+} ions formed and the overall conduction, since electron transfer between Ni^{2+} and Cr^{3+} or Al^{3+} does not occur.

Similar defect mechanisms can be expected in other oxide systems which exhibit both n- and p-type conduction. For example, Fe_2O_3 is an n-type semiconductor under conditions where oxygen ion vacancies are formed, with charge compensating electrons localized on the cation sites. This is the equivalent of forming Fe^{2+} ions on Fe^{3+}sites, resulting in electron polaron hopping and increased conduction. If Ti^{4+} is added to Fe_2O_3 in solid solution, an increased fraction of Fe^{3+} ions are forced into the Fe^{2+} state. As a result, the conductivity of the oxide substantially increases, ranging from 10^{-10} to $10^{-2}(\Omega\text{-cm})^{-1}$ for an added Ti^{4+} concentration of zero to 0.5 atom %. Again, conduction is determined primarily by the concentration of added titanium ions and is much less dependent on oxygen partial pressure and firing conditions. Tin oxide, SnO_2, and indium oxide [1312-43-2] In_2O_3, are other important oxides that are doped to increase conductivity. The SnO_2, In_2O_3, TiO_2, and in particular, $SrTiO_3$, are transparent to visible light and are often used as transparent electrodes, eg, on Vidicon tubes (Table 5).

Titanium dioxide as a semiconductor material is used as a gas sensor, and is sensitive to changes in ambient oxygen partial pressure. Whereas in the electrochemical sensor, $ZrO_2{\cdot}Y_2O_3$, conduction is by oxygen ions, in TiO_2 sensors the conduction is by electrons (36). Pure TiO_2 has a band gap of 3.2 eV, and a fully occupied oxygen 2*p* valence band (27). Therefore, at room temperature it is a highly resistive material. At elevated (>500°C) temperatures, depending on oxygen partial pressure, it becomes oxygen deficient and Ti^{3+} ions are formed to compensate for the anion deficiency, along with mobile electrons. As more oxygen vacancies are created, the electron concentration increases and the resistivity decreases. Resistivity in these materials is, therefore, highly dependent on temperature, formation energy for the oxygen vacancies and on oxygen partial

Table 5. **Impurity Semiconductors**

		n-Type			
Cds	$BaTiO_3$	Nb_2O_5	Fe_2O_3	WO_3	GeO_2
CdSe	$SrTiO_3$	Ta_2O_5	Tl_2O_3	TiO_2	MnO_2
ZnF_2	$PbCrO_4$	Fe_3O_4	In_2O_3	SnO_2	ZnO
		p-Type			
Se	CuI	Ag_2O	Hg_2O	NiO	PdO
Te	SnS	Cu_2O	MnO	FeO	CoO
		Amphoteric			
Si	Sn	PbSe	Ti_2S	Al_2O_3	Mn_3O_4
Ge	PbS	SiC	PbTe	Co_3O_4	UO_3

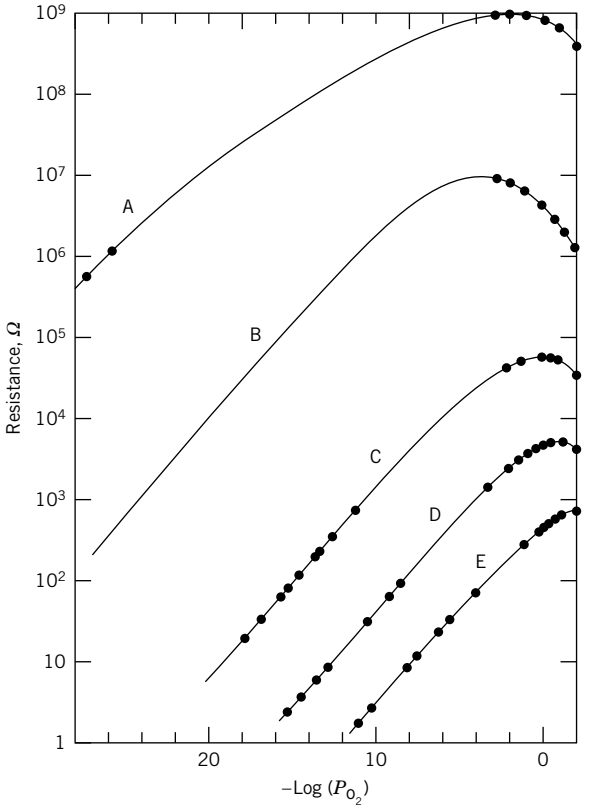

Fig. 4. Dependence of the resistance of TiO_2 ceramics on oxygen partial pressure in kPa. A, at 320°C; B, at 500°C; C, at 700°C; D at 850°C; and E, at 1000°C. To convert kPa to psi, multiply by 0.145 (36).

pressure, as shown in Figure 4 (36). This oxygen pressure dependence for many oxides is of the form: $\sigma = {P_{O2}}^{\pm\delta}$, where δ has values typically ranging from $\pm$ 1/8 to 1/2. The sign of δ indicates p-type (+); or n-type (−) conduction.

Another method for obtaining semiconductors with controlled resistivities, which avoids the difficulties caused by stoichiometric deviations, is by solid solution of two or more compounds with widely different conductivities. Magnetite [1317-61-9], Fe_3O_4, is an excellent conductor having a specific resistivity of $\sim 10^{-4}$ Ω-cm at room temperature, compared to resistivities of $\sim 10^8$ Ω-cm for most stoichiometric transition-metal oxides. The high electrical conductivity of magnetite is a function of the random distribution of Fe^{2+} and Fe^{3+} ions on octahedral sites, allowing for easy electron transfer between cations. This is best illustrated by the order–disorder transformation occurring at ~120 K. Below this temperature the Fe^{2+} and Fe^{3+} ions are distributed in an ordered pattern on the octahedral sites. Above this temperature Fe^{2+} and Fe^{3+} positions become randomly distributed, resulting in a substantial increase in conductivity.

9. Spinels Ferrites

The spinel crystal structure (AB_2O_4) is based on the cubic close packing of oxygen ions in which the cations are situated on both the tetrahedral A and octahedral B sites (8,37). In spinel ferrites for magnetic applications, cations such Fe^{3+} or Mn^{2+} can occupy both A and B sites, giving an inverse [$(AB)BO_4$] structure and higher net magnetization. In the spinel lattice, the normal cations such as Ni, Co, Li, Mg, Zn, Cd, etc show a definite preference for either the tetrahedral or octahedral sites. The cation concentration and site preference essentially determines the properties of the ferrite. Ferrites need to have high electrical resistivities in order to eliminate eddy current and dielectric losses, as well as for allow full penetration of electromagnetic fields throughout the solid (38,39). High resistivity is obtained when a cation has only one valence state in the lattice. In the processing of these materials, therefore, high sintering temperatures and reducing atmospheres must be avoided since these conditions can produce variable valence states on some cations. The range of published resistivities for spinel and garnet [12178-41-5] ferrite materials is wide, from $\sim 10^{-4}$ to $10^9 \Omega$-cm at room temperature (38,39). The low conductivity is typically associated with the simultaneous presence of Fe^{2+} and Fe^{3+} ions on equivalent lattice sites. In general, a condition for appreciable conductivity in the ferrite structure is the presence of ions having multiple valence states on like crystallographic sites. Thus, the concentration of ions in Fe_3O_4 can be controlled by solid solution in which Fe^{2+} or Fe^{3+} are diluted by other ions that do not participate in the electron exchange.

There are three main commercial classes of ferrite spinels, namely: nickel–zinc ferrite, $(NiZn)Fe_2O_4$; manganese–zinc ferrite, $(MnZn)Fe_2O_4$; and, magnesium–manganese ferrites, $(MnMg)Fe_2O_4$. The electrical conduction is by small polaron mechanisms. Electrical resistivity primarily determines the utility of these materials in the high megahertz or microwave frequency ranges. Low frequency use requires a trade-off between high permeability and high resistivity. Nickel–zinc ferrites typically show an increase in permeability and a departure from stoichiometry in the iron-rich direction. Decreased resistivity results, therefore, when the formation of divalent iron becomes more probable, requiring close control of processing parameters is. Manganese–zinc and magnesium–manganese zinc ferrites are typically used in low frequency devices such as pulse transformers and memory-core devices. For higher frequency use, the high dc resistivity needed for full magnetic penetration and low eddy current losses can be obtained with an iron deficient oxide powder. However, a more complex processing situation arises because of the three possible valence states of manganese cation and the site preference for each. Sintering temperature and cooling rate can also impact the magnesium site locations. Increasing the amount of manganese increases the lattice constant, making it easier for the Mg ions to occupy both cation sites, such that divalent and trivalent ions are present on both sites, with adverse impact on the permeability, resistivity, and utility of the material (37,39).

Information regarding solid solutions of Fe_3O_4 and $MgCr_2O_4$, hercynite [1302-61-0], $FeAl_2O_4$, and ferrous chromite [1308-31-2], $FeCr_2O_4$, have been published (38). Semiconductor materials of this type, with controlled temperature

coefficient of resistivity, have been prepared using materials such as $MgAl_2O_4$, $MgCr_2O_4$, and titanium zinc oxide [12036-69-0], Zn_2TiO_4, as the nonconducting component. Semiconductors made in this way are used as thermistors. Because the electrical conductivity the semiconductors made in this way have a negative temperature coefficient (NTC), these materials are typically utilized in temperature sensing and thermistors applications. Copper–nickel manganites, $Mn_{3-x-y}Ni_y\ Cu_xO_4$ spinels, are of technological importance for use in very low resistance thermistors (8). Through adjustment in stoichiometry, the electrical conductivity can increase to 0.1 $(\Omega = \text{cm})^{-1}$ at room temperature. In nickel–manganites the conduction is primarily through electron hopping from Mn^{3+} to Mn^{4+} cations on the B sites. In the copper–nickel–manganites the situation is quite complex since there is the presence of Ni^{2+}, Mn^{2+}, Mn^{3+}, and Mn^{4+} ions as well, hence, there is uncertainty over distribution of copper cations and their ionic states.

10. Superconductivity

Oxide superconductors have been known since the 1960s. Compounds such as niobium oxide [12034-57-0], NbO, TiO, $SrTiO_{3-x}$ and AWO_3, where A is an alkali or alkaline earth cation, were found to be superconducting at 6 K or below. The highest T_c observed in oxides before 1986 was 13 K in the perovskite compound $BaPb_{1-x}\ Bi_xO_3$, for $x = 0.27$. Then in 1986 possible superconductivity at 35 K in the La–Ba–Cu–O compound was discovered (40). The compound was later determined to be $La_{1.85}\ Ba_{0.15}\ CuO_4$. Work on the Y–Ba–Cu–O system was published in 1987 with a reported a transition temperature above 90 K (41). This transition temperature was surpassed in early 1988 by the discovery of a series of bismuth-containing compounds, Bi–Sr–Ca–Cu–O, having the highest $T_c = 100$ K, and a $Tl_2\ Ba_2\ CaCu_2O_{8-y}$ compound having a $T_c = 120$ K (42,43) (see BISMUTH COMPOUNDS).

Superconductivity is partly typified by a perfect metallic conductor that has no resistance to current flow below a T_c. Besides the disappearance of electrical resistance, there is an expulsion of magnetic flux described as the Meissner effect. The widely acclaimed BCS theory explains traditional superconductivity based on the concept of Cooper pairs. The Cooper pairs are formed when electrons interact with phonons and attract each other, resulting in a combined energy state that is lower than the Fermi energy of the normal conduction electrons. These Cooper electron pairs move in such a way that at equilibrium the combined momentum is unchanged. Normal scattering effects, therefore, do not affect the forward momentum of the electrons accelerating in an electrical field. In spite of the success of the BCS theory for low temperature superconductors, the high temperature oxide superconductors do not conform well to the prediction of this model. Specifically, the BCS theory does not predict a $T_c >$ 30 K or the existence of a weak or no isotope effect. Any theory must consider the local charge inhomogeneities as well as the local electronic structure at distances of the order of the superconducting coherence length. Research studies aimed at understand the superconducting phenomenon in oxide systems and

also increasing the transition temperature, have resulted in a large volume of literature on the subject.

A model by Emery and Kivelson (18) considers high temperature superconductors to be quasi-two dimensional doped insulators, obtained by chemically introducing charge carriers into a highly correlated antiferromagnetic insulating state. The model interprets the transition temperature as being inversely proportional to the spacing of one-dimensional arrays or stripes that are formed in the under-doped and optimally doped materials. In the under-doped insulating state, there exist charge inhomogeneities that are also antiphase domain walls for the background spins. The superconducting state is featured as a 2D array comprising rivers of charges flowing through the antiferromagnetic bulk, separating the background spins into loosely coupled regions (18). Another model proposed by Hirsch (19) states that only hole carriers in a solid can produce superconductivity, and that the negative charges will be expelled from the bulk and move to the surface, leaving the interior positively charged. In this theory the holes are expected to pair and have a smaller effective mass, becoming superfluid carriers. With this, there is an associated lowering of the kinetic energy that provides the superconducting condensation energy (19). Both the weak coupling and the strong coupling approaches described, can lead to the energy perturbation condition that triggers the superconducting state (17).

The $YBa_2\ Cu_3O_{7-x}$ compound is currently the most intensively investigated high temperature oxide superconductor. It has an oxygen deficient, distorted orthorhombic, 1:1:3 (ABO_3) perovskite-type structure, with the *Pmmm* space group (45). The crystal structure shows the Y and Ba ions located in the center of the unit cell, Cu ions on the corners, and O ions on the edges. Based on neutron diffraction studies, the structure shows two important features for the Cu ions: (*1*) nonplanar CuO_2 planes extend in the crystallographic *ab* planes at $z = 0.36$ and -0.36; and (*2*) fencelike, square planar CuO_3 linear chains extending along the *b* axis at $z = 0$. CuO_2 layers appear in all cuprate superconductors and seem to be a necessary but not sufficient condition for high temperature superconduction to occur (46). The $La_2\ SrCu_2O_{6.2}$ compound has CuO_2 layers but does not superconduct. Studies also indicate that T_c is proportional to the carrier density in the CuO_2 layer but not to the volume carrier density, which is further evidence that the $YBa_2\ Cu_3O_{7-x}$ is a 2D superconductor. In these materials, the electrical conductivity and critical fields are highly anisotropic. Figure 5 shows this for highly oriented films and the single crystal in two directions (47). Conductivity in the *ab* (CuO) planes is metallic, whereas along the *c* axis it is semimetallic. The conductivity can be greatly disturbed by defects such as vacancies and twin boundaries, in which the *a* and *b* axes are reversed, in particular by grain boundaries in the polycrystalline material. Because of the severe anisotropy, the critical current density is much higher in the plane than along the *c* axis.

The $YBa_2Cu_3O_{7-x}$ oxide superconductor is called an oxygen deficient perovskite because there are only seven oxygens per formula unit instead of the nine oxygens required for a perfect perovskite. The oxygen content in this compound is thus sensitive to processing and annealing conditions. When the *x* value is <0.5, an orthorhombic superconducting phase is present. As the compound loses oxygen and *x* becomes >0.5, an order–disorder phase transition occurs

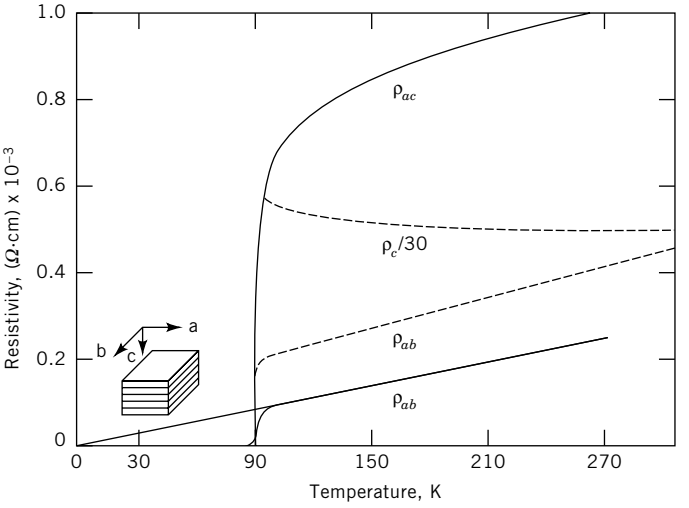

Fig. 5. Resistivity versus temperature showing onset of superconductivity for a single crystal (- - -) and for two highly oriented films (—), where ρ_{ab} denotes resistivity in the *ab* plane, ρ_{ac} in the *ac* plane, and $\rho_c/30$ represents 1/30 the resistivity in the *c*-direction to account for the much higher resistivity in this direction (47).

and the structure transforms to a tetragonal phase having semiconducting characteristics. The tetragonal phase has a $P4/mmm$ space group with oxygen disordered in the $z = 0$ planes, compared to the orthorhombic phase. There is a volume change of $+0.2\%$ associated with this phase transformation. Therefore, stresses are present resulting from the transformation and cause a twin structure formation, usually observed along the (110) reflection planes. The twin structure does not interrupt the continuity of the Cu−O superconducting planes, but does terminate the Cu−O chains between the Ba and Y planes.

The wide transition temperatures are found to be strongly dependent on oxygen stoichiometry. The high transition temperature at 92 K in this compound can only be obtained when the oxygen content is between 6.8 and 7.0. Although T_c generally decreases as the oxygen content is reduced, the exact relationship depends critically on the processing conditions. Applications for superconductors include magnetic resonance imaging for medical diagnostics (see IMAGING TECHNOLOGY), particle accelerators for experimental physics, and superconducting quantum interference devices (SQUID).

11. Ferroelectrics

Barium titanate, $BaTiO_3$, has been a much studied ferroelectric, since it is the base material for large volume production of technologically important components such as disk and multilayer (MLC) capacitors; barrier layer (BL) and grain boundary barrier layer capacitors (GBBL); and, nonlinear PTCR. Barium titanate has a tetragonal structure over the range of ~5–125°C, with the dielectric constant rising to a peak near the critical transition temperature of ~125°C,

defined as the Curie temperature, T_C. The ferroelectricity in $BaTiO_3$ and like (ABO_3) perovskite compounds arises from a dipolar shift in the B cations on cooling through the transition temperature. This results in a change in crystal symmetry from cubic to tetragonal and the appearance of spontaneous polarization charges (16), due to the development of a domain structure. Domains are unipolar regions within the crystal which, in the absence of an externally applied field, are randomly aligned so as to exhibit no net internal polarization. Above the Curie temperature, the material reverts to the nopolar state with disappearance of the spontaneous polarization (4,5,21,22).

$BaTiO_3$ has an intrinsic high resistivity of $\sim 10^{10}$ Ω-cm, when prepared in an oxidizing atmosphere. However, it can readily become semiconducting (48) through controlled doping of the A-site lattice using La^{3+}, Y^{3+}, or Nd^{3+}, or of the B-sites using Nb^{5+}or Ta^{5+} and like cations. A complex defect structure can result from the presence of different charge compensation mechanisms as the dopant level is increased. At low dopant concentration (0.1–0. 3 mol%), n-type conduction results, due to the formation of donor level Ti^{3+} ions with mobile electrons (48,49). At higher dopant levels, the mechanism changes from electronic to ionic compensation, due to cation vacancy formation, leading to a significant increase in resistivity (50,51). Low resistivities are obtained only within a very narrow dopant concentration range of ~0.1–0.3 mol%. The formation of the Ti^{3+} ions in the doped $BaTiO_3$ lattice, leads to local distortion of the TiO_6 octahedra, causing a change in the polarization field and a lowering of the Ti(3*d*) energy level associated with the Ti^{3+} state. Intermediate polaron conduction occurs due to the splitting of the Ti(3*d*) orbitals (15,16). The mode of conduction results, therefore, from polarization field overlap of the localized Ti^{4+} and Ti^{3+} discrete energy levels, aided by the lattice distortion caused by the electron movement and change in Ti valence state.

Under controlled heat treatment, a thin, insulating grain boundary layer can be formed in the polycrystalline ceramic. In this grain boundary region oxygen is adsorbed during annealing, reducing the Ti^{3+} concentration (27). Oxygen vacancies may also diffuse from the interior to the grain boundary region where they act as electron traps. A space charge or barrier layer is thereby formed which repel electrons moving towards the grain boundary. Studies of this near-grain boundary region in doped and annealed $BaTiO_3$ samples show these to be regions of high strain, with defect segregation and a domain structure that is different from the interior (52,53). In contrast, the nonannealed materials feature only limited segregation, low strain and a near uniform domain structure. For the annealed material, a martensitic-type transformation or structure change within the narrow grain boundary region, coupled with the sudden release of stress, is considered to be the driving force for the abrupt change in grain boundary potential and resistivity that is observed (52,53). At temperatures below the critical ferroelectric phase transition, (+) spontaneous polarization charges can neutralize the (−) grain boundary charges in crystallographically coherent areas along the grain boundaries, creating thereby a low resistance pathways (52–55) and significantly lower ressistivity overall. In *n*-doped $BaTiO_3$, PTCR behavior is observed as a large increase in resistance (typically, several orders of magnitude) near the phase transition temperature over a narrow range of dopant concentration. Both the PTCR effect and room

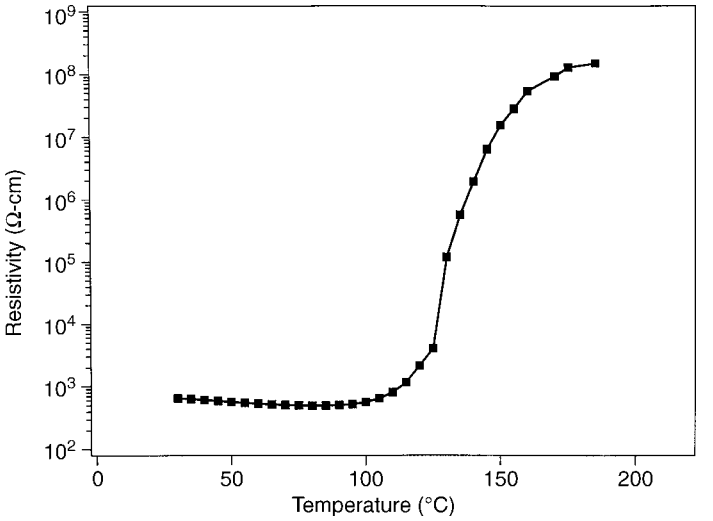

Fig. 6. PTCR resistivity–temperature characteristics for donor modified barium titanate.

temperature resistivities are highly dependent on dopant type and ionic radius. Figure 6 is a resistivity–temperature plot of a typical PTCR behavior, showing a low resistivity region and a sharp increase in resistivity near the ferroelectric phase transition. Materials with this type behavior are used for current limiting, temperature control, resistive heating, motor starters, and for sensor applications.

Barrier layer capacitors having high dielectric constants and low losses can be produced by increasing the grain boundary thickness through the use of additional dopants, such that the grain boundary barrier layer becomes impassable to electrons, by creating a large concentration of acceptor states that nullify the effects of the spontaneous polarization. This traps the conducting electrons by creating a space charge layer, which repels like charges. Several additional dopants, eg, Sr, Zr, Pb, Si, Cu, and Bi, to $BaTiO_3$-based systems are used in the manufacture of both capacitor and PTCR sensor devices, in order to adjust the switching temperature and other operating characteristics.

Perovskites with Pb on the A site are particularly important and show pronounced piezoelectric characteristics ($PbTiO_3$, PZT, PLZT). Different responses are found in $BaTiO_3$ and PZT to the addition of donor dopants such as La^{3+}. In PZT, lead monoxide [1317-36-8], PbO, which is partially lost by volatilization during sintering, can be replaced in the crystal by La_2O_3, where the excess positive charge of the La^{3+} is balanced by lead vacancies, giving ionic compensation and no generated electronic charge carriers (4). This results in a marked increase in resistivity of the material. Relaxors materials show a significant change in permittivity with frequency at temperatures near the Curie point, T_C. These materials also exhibit high permittivity values near T_C. Of particular interest for capacitors use are the lead-based relaxors having the general formula $Pb(B_1B_2)O_3$, where B_1 is typically a low valence cation (Mg, Zn, Fe, Ni, or Sc), and B_2 is a high valence cation (Ti, Nb, Ta, or W). The best known relaxor

formulations are in the $Pb(Mg_{1/3}\,Nb_{2/3})O_3$ system (PMN), which shows excellent relaxor characteristics with a combined high dielectric permittivity and high resistivity. These lead-based materials (PZT, PLZT, PMN) form a class of ceramics with important dielectric, relaxor, piezoelectric, or electrooptic properties, and are thus used for actuator and sensor devices. Common problems associated with their use are low dielectric breakdown, increased aging and electrode injection, thereby decreasing the resistivity and degrading the dielectric properties (4).

12. Varistors

Varistors are primarily ZnO-based ceramic devices, which exhibit high nonlinear current–voltage behavior, which is ideal for use in protecting electronic equipment against voltage surges. To obtain the appropriate current–voltage characteristics, the polycrystalline ZnO is usually doped with antimony(III) oxide [1309-64-4], Sb_2O_3, bismuth(III) oxide [1332-64-5], Bi_2O_3, and like additives. The material is then processed so as to develop a microstructure consisting of conductive grains surrounded by a thin, resistive, Bi-rich second phase in the grain boundaries (56). This microstructure can be quite complex and is key to understanding the barrier layer conduction behavior in varistors. At low voltages the grain boundary resistance is sufficiently high that little current leaks from the circuit. At the higher breakdown voltages a tunneling process occurs, which allows the overvoltage pulse to be rapidly gated away from the device circuitry. This is because the varistor resistance to ground decreases several orders of magnitude (Fig. 7), similar to the PTCR devices previously described, although the actual operating mechanism is very different (56). Figure 7 shows the current density J versus applied field E for a typical varistor, in which the shape of the curve is largely defined by the slope **a**. A large variation in current density is seen for a comparatively small change in the field, which is a significant advantage for ZnO varistor use. Because the varistor action takes place across the ZnO

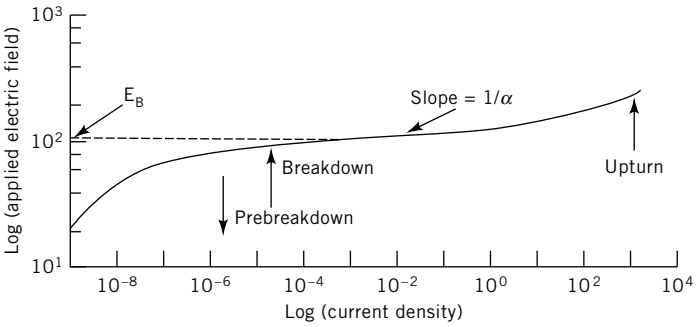

Fig. 7. Log–log plot of current density, J, versus applied electric field, E, for a ZnO varistor at room temperature, in which the breakdown field, E_B, is indicated. The exponent α equals the inverse slope of the curve, $\log(E/J) = 1/\alpha$, and is a measure of device nonlinearity. Units of current density and the electric field are A/cm^2 and V/cm, respectively (56).

grain boundaries, the tailoring of devices for specific breakdown voltages is done by fabricating the device with the appropriate number of grain boundaries in series between the electrodes. The current density /voltage behavior can be described by a power law:

$$I = k\mathrm{V}^{\alpha} \ (1 \leq \alpha \leq \infty) \tag{20}$$

where I is the current through the device, V is the voltage, and the exponent α, which is a measure of device nonlinearity, is typically in the range 20–50. Ohmic-type behavior is usually found for low values of α (ie, for $\alpha \sim 1$), whereas varistor behavior is typically attained for values of $\alpha > 20$.

More recently, a different role has been ascribed to the grain boundary phase in current flow regulation. Here, the conductive grains are considered to be separated by a thin, adsorbed oxide layer that stores a negative charge equal in magnitude to the positive charge in the depletion layer, which lies wholly within each grain near the grain boundaries. These depletion regions are believed to create a barrier to electron flow at low voltages. Transport through the grain junction becomes then a compound step process. As the voltage increases, the depletion layer thins because there is a dramatic change in the conduction band shape and long-lived holes appear in the valence band. Electrons are able to tunnel through the interface because the tunneling barrier is now much thinner, and current flow becomes greatly enhanced (56).

In any event, it is clear that the state of the grain boundary region is the critical factor in determining device performance in both PTCR and varistor type devices. Depletion regions in the near grain boundary area are usually electonically active, since they act as barriers to charge flow. Thereby, it controls electronic and mixed conduction, as well as contributes to space charge polarization and high permittivity in these electroceramic systems. Understanding of the conduction phenomenon in these type materials is more complex than a simple description of depletion regions, however, since dopant effects, grain boundary and mechanical states also significantly affect conduction (6,57). The mechanical states can be described in terms of misorientation of adjacent grains and density of coinciding sites (sites that belong to the lattice of both grains). It affects, therefore, the coherency of the grain boundary and stress states. The combined mechanical and charge effects lead to depletion or accumulation effects for the mobile ionic and electronic charges. The grain boundary depletion or space charge layers are often described as back-to-back Schottky barriers, in which the width of the disruption region controls the properties (6,7,46,56,57). Since processing effects (including doping and heat treatment) have the potential to create and control grain boundary states, their impact on electrical properties can be substantial.

13. Processing Effects

Electrical ceramic properties are ultimately structure dependent, especially in those ceramic materials with variable valence cations. The processing of these

materials, therefore, require close control of composition and heat treatment conditions. Microstructure and grain size control are also crucial since density changes and the presence of second phases can grossly affect properties. Thermal history during processing can affect properties in important ways as well. For example, in ferrite ceramics such as $MgFe_2O_4$, the distribution of cations between octahedral and tetrahedral sites determines magnetic behavior, but this site occupancy can be significantly altered by heat treatment and cooling rate. Rapid cooling from the sintering temperature, for instance, can cause development of a net magnetic moment in normally nonmagnetic Mg or even Zn ferrite.

Conducting ceramics based on nanocrystalline powders are of interest for use in electrochemical and catalytic systems and as photocatalysts. For many of these applications, the influence of density of grain boundaries on conductivity is not well understood, although it is known that grain size strongly influences conductivity in important material systems such as CeO_2, SnO_2, and ZrO_2 (59). The size dependence may be related to the development of space charge effects as the grain size approaches the Debye length (59). For example, the sensitivity of a porous SnO_2 gas sensor strongly increases when the grain size becomes comparable to the width of the space charge layer. In this state the entire grain can be considered depleted of electrons in the nonsensing condition. The dc conductivity in nanocrystalline TiO_2 is also enhanced relative to the coarse grain material. Nanocrystalline CeO_2 also shows a lower specific grain boundary resistivity than the coarse-grained material. The behavior, in this case, has been attributed to size dependent grain boundary impurity segregation. With increasing grain boundary area, due to smaller grains, the grain boundary impurity concentration decreases. This leads to a lower blocking effect on conduction electrons and ions and a correspondingly lower grain boundary resistivity (59). Grain boundary segregation and nonstoichiometry effects also impact electrical behavior in these nanostructured materials.

The effect of grain size on ionic and on mixed ionic-electronic conducting ceramics is also of interest, particularly for solid oxide fuel cells (SOFC) (57). Oxygen-ion conductors such as stabilized zirconia, ceria and lanthanum gallate, are promising systems for use as solid electrolytes. For long-term use and stability, the SOFCs need to operate at $\sim 750^{\circ}C$ or below, but this requires a corresponding increase in electrolyte conductance and in gas–electrode reaction kinetics, parameters which typically decrease with operating temperature. The use of nanocrystalline materials can be advantageous for these type applications, if the ionic conduction along grain boundaries can be enhanced with the nanosized grains. This is because grain boundary diffusion is significantly greater than bulk diffusion, due to higher defect densities and mobilities in the disordered grain boundaries (57). Space charge effects may also develop, which repel like charges, leading to an accumulation of opposite charges along the grain boundary. If these opposite charges became mobile, ionic conduction along the grain boundary would be enhanced. Studies into enhanced ionic conductivity in nanosized crystalline materials have thus far been inconclusive, since enhanced electronic conductivity often masks changes in ionic conductivity, as, eg, in CeO_2. In designing electrical ceramics for particular applications, therefore, processing parameters must be carefully monitored and controlled.

BIBLIOGRAPHY

"Ceramics as Electrical Materials" in *ECT* 3rd ed., Vol. 5, pp. 290–314, by H. Kent Bowen, Massachusetts Institute of Technology; in *ECT* 4th ed., Vol. 5, pp. 698–728, by R. C. Buchanan and R. D. Roseman, University of Illinois, Urbana-Champaign; "Ceramics as Electrical Materials" in *ECT*, (online), posting date: December 4, 2000, by R. C. Buchanan and R. D. Roseman, University of Illinois, Urbana-Champaign.

CITED PUBLICATIONS

1. R. Waser, *J. Eur. Ceram. Soc.* **19**, 655 (1999).
2. R. E. Newnham, *Rep. Prog. Phys.* **52**, 123 (1989).
3. Y. Chiang, D. Birnie, and W. D. Kingery, *Physical Ceramics*, John Wiley & Sons, Inc., New York, 1997.
4. A. J. Moulson and J. M. Herbert, *Electroceramics*, Chapman and Hall, New York, 1990.
5. R. C. Buchanan, ed., *Ceramic Materials for Electronics*, 2nd ed., Marcel Dekker, Inc., New York, 1991.
6. R. Waser and R. Hagenbeck, *Acta Mater.* **48**, 797 (2000).
7. G. Garcia-Belmonte, J. Bisquert, and F. Fabregat-Santiago, *Solid State Electron.* **43**, 2123 (1999).
8. E. Elbadraoui, J. L. Baudour, F. Bouree, B. Gillot, S. Fritsch, and A. Rousset, *Solid State Ionics* **93**, 219 (1997).
9. G. Chiodelli, G. Flor, and M. Scagliotti, *Solid State Ionics* **91**, 109 (1996).
10. V. V. Kharton, A. P. Viskup, D. M. Bochkov, E. N. Naumovich, and O. P. Reut, *Solid State Ionics* **110**, 61 (1998).
11. H. Ullmann, N. Trofimenko, A. Naoumidis, and D. Stover, *J. Eur Ceram. Soc.* **19**, 791 (1999).
12. J. J. Sprague and H. L. Tuller, *J. Eur Ceram. Soc.* **19**, 803 (1999).
13. D. Basak and J. Ghose, *J. Solid State Chem.* **112**, 222 (1994).
14. G. Blaise, *J. Electrostat.* **50**, 69 (2001).
15. V. V. Paranjape and P. V. Panat, *J. Phys.: Condens. Matter.* **3**, 2319 (1991).
16. I. Bunget and M. Popescu, in C. Laird, ed., *Materials Science Monographs*, Vol. 19, Elsevier, Amsterdam, The Netherlands, 1978, Translation, V. Vasilescu, 1984.
17. J. R. Schrieffer, *Physica B*, 259–261 433 (1999).
18. V. J. Emery and S. A. Kivelson, *J. Phys.* / Chem. Solids **61** 467 (2000).
19. J. E. Hirsch, *Phys. Lett. A* **281**, 44 (2001).
20. N. M. Tallen, ed., *Electrical Conductivity in Ceramics and Glasses*, Marcel Dekker, Inc., New York, 1974.
21. D. W. Richerson, *Modern Ceramic Engineering*, 2nd ed., Marcel Dekker, Inc., New York, 1992.
22. L. L. Hench and J. K. West, *Principles of Electronic Ceramics*, John Wiley & Sons, Inc., New York, 1990.
23. E. C. Subbarao, ed., *Solid Electrolytes*, Plenum Press, New York, 1980.
24. V. Z. Kresin and S. A. Wolf, eds., *Fundamentals of Superconductivity*, Plenum Press, New York, 1990.
25. R. Wernicke, in *Ceramic Monographs-Handbook of Ceramics*, Suppl. Interceram. Vol. 34(6), No. 3.1.5, 1985.
26. V. V. Kharton, A. P. Viskup, A. V. Kovalevsky, J. R. Jurado, E. N. Naumovich, A. A. Vecher, and J. R. Frade, *Solid State Ionics* **133**, 57 (2000).

27. D. C. Hill and H. L. Tuller, in R. C. Buchanan, ed., *Ceramic Materials for Electronics*, 2nd ed., Marcel Dekker, Inc., New York, 1991.
28. G. Fisher, *Am. Ceram. Soc. Bull.* **65** (4), 622 (1986).
29. H. L. Tuller, in Ref. 5.
30. R. C. Buchanan, in Ref. 5.
31. H. Cordes and S. D. Baranovskii, *Phys. Status. Solids B* **218**, 133 (2000).
32. C. H. Hsieh and H. Jain, *J. Non-Crystalline Solids* **183**, 1 (1995).
33. H. Kahnt, *J. Non-Crystalline Solids* **203**, 225 (1996).
34. M. F. Yan and A. H. Heuer, eds., in *Advances in Ceramics*, Vol. 7, American Ceramic Society, Columbus, Ohio, 1982.
35. W. Williams, *Inter. J. Refract. Metals Hard Mater.* **17**, 21 (1999).
36. E. M. Logothetis, *Ceram. Eng. Proc.* **1**, 281 (1980).
37. F. N. Bradley, in A. E. Javitz, ed., *Materials for Magnetic Functions*, Hayden Book Co., Inc., New York, 1971.
38. E. J. Verway, P. W. Haagman, and F. C. Romeijn, *J. Chem. Phys.* **15**, 18 (1947).
39. K. J. Standley, *Oxide Magnetic Materials*, 2nd ed., Clarendon Press, Oxford, UK, 1972.
40. J. G. Bednorz and K. A. Muller, *Z. Phys. B-Condensed Matter* **64**, 189 (1986).
41. M. K. Wu and co-workers, *Phys. Rev. Lett.* **58**(9), 908 (1987).
42. H. Maeda, Y. Tanaka, M. Fukutomi, and T. Asano, *Jpn. J. Appl. Phys.* **27**(2), L209 (1988).
43. Z. Z. Sheng and A. M. Hermann, *Nature. (London)* **332**, 138 (1988).
44. J. Bardeen, L. H. Cooper, and J. R. Schrieffer, *Phys. Rev.* **106**, 162 (1957).
45. M. A. Beno and co-workers, *Appl. Phys. Lett.* **51**(1), 57 (1987).
46. K. Mukae and A. Tanaka, *Ceramics Inter.* **26**, 645 (2000).
47. B. Kulwicki, in L. Levinson, ed., *Grain Boundary Phenomena in Electronic Ceramics, Advances in Ceramics.*, Vol. 1, 1981, pp. 138–154.
48. W. Heywang, *J. Mater. Sci.* **6**, 1214 (1971).
49. G. H. Jonker, *Solid State Electron.*. **1**, 895 (1964).
50. K. Takada, E. Chang, and D. M. Smyth, in J. B. Blum and W. R. Cannon, eds., *Multilayer Ceramic Devices, Advances in Ceramics.*, Vol. 19, 1987 pp. 147–51.
51. J. Kim, R. D. Roseman, R. C. Buchanan, and *Ferroelectrics* **177**, 255 (1996).
52. R. D. Roseman, and J. Kim, R. C. Buchanan, *Ferroelectrics* **177**, 273 (1996).
53. R. D. Roseman, *Ferroelectrics* **215**, 31 (1998).
54. R. D. Roseman and G. Liu, *Ferroelectrics* **221**, 181 (1999).
55. L. M. Levinson and H. R. Philipp, in Ref. 12.
56. H. Tuller, *Solid State Ionics* **131**, 143 (2000).
57. T. H. Geballe and J. K. Hulm, *Science* **239**, 367 (Jan. 22, 1988).
58. M. Takemoto, T. Miyajima, K. Takayanagi, T. Ogawa, H. Ikawa, and T. Omata, *Solid State Ionics* **108**, 255 (1998).
59. C. Demetry and X. Shi, *Solid State Ionics* **118**, 271 (1999).

RELVA C. BUCHANAN
RODNEY D. ROSEMAN
University of Cincinnati